HHS Public Access

Author manuscript

J Control Release. Author manuscript; available in PMC 2016 December 28.

Published in final edited form as:

J Control Release. 2015 December 28; 220(0 0): 245–252. doi:10.1016/j.jconrel.2015.10.036.

Comparative Effect of Gold Nanorods and Nanocages for Prostate Tumor Hyperthermia

Ryan Robinson[a,b], **Wiebke Gerlach**[b,c], and **Hamidreza Ghandehari**[a,b,c,*]

[a]Department of Bioengineering, University of Utah, Salt lake City, UT, 84112, USA

[b]Center for Nanomedicine, Nano Institute of Utah, Salt lake City, UT, 84112, USA

[c]Department of Pharmaceutics and Pharmaceutical Chemistry, University of Utah, Salt lake City, UT, 84112, USA

Abstract

Gold nanoparticles have been investigated as photothermal agents, drug delivery carriers, diagnostics, and theranostics. As long-term accumulation of nanoparticles in nontarget tissues is a growing concern, it is vital to establish biodistribution profiles, tumor uptake, and tissue residence times for each nano-based system. This study aimed to investigate the prostate tumor uptake, photothermal therapy mediated macromolecular delivery, acute and chronic biodistribution profiles, and organ residence time differences between two nanoparticles, i.e., gold nanocages and gold nanorods. These particles have tunable surface plasmon resonances in the near infrared, but dissimilar shapes. Gold nanocages and nanorods had very different light to heat transduction efficiencies, with gold nanocages requiring 18.4 times fewer particles and approximately half the gold mass of gold nanorods to achieve the same heating profile given a constant laser intensity. It was also observed that while the photothermal macromolecular delivery enhancements were similar for the two systems when dosed by optical density, the tumoral uptake and biodistribution profiles for each of these shapes differed, with the nanocages residing in the liver, kidneys and spleen for less time than the nanorods. Additionally, it was observed that the nanocages were excreted from the body at a higher percentage of injected dose than the nanorods at both the 7 and 28 day time points. These findings have implications for the use of these constructs in diagnostic and therapeutic applications.

Graphical abstract

[*]Corresponding author. hamid.ghandehari@pharm.utah.edu, Ph: 801-587-1566, Fax: 801-585-0575, Address: 36 S. Wasatch Dr., Salt Lake City, UT, 84112-5001.

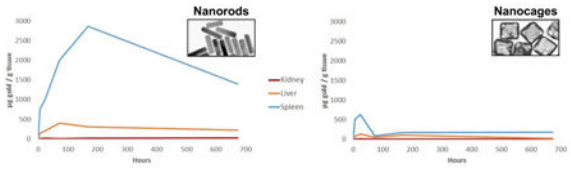

Keywords

Gold nanocages; gold nanorods; photothermal therapy; hyperthermia

1. Introduction

Advances in the synthesis and characterization of gold nanoparticles have led to an expanded control over shape, size, and surface chemistry. This has resulted in an array of work exploring the applications of plasmon-resonant nanoparticles in the treatment and diagnosis of malignancies [1-3] Prostate cancer is the second most common cancer, and the second leading cause of cancer related death in American men [4]. Localized prostate cancer accounts for 81% of these cases and the most common current methods of treatment are surgery and radiation therapy, together accounting for 90% of all treatments [4, 5]. Prostate cancer yearly expenditures exceed $12 billion in treatment costs in the United States [6, 7]. In addition to the high associated cost, current therapies are often time intensive and painful for the patient. Replacing current treatment methods with photothermal therapy could provide significant financial savings, cut down treatment time, and alleviate patient discomfort [8].

Plasmonic photothermal therapy (PPTT) is an efficient method of inducing localized hyperthermia using electromagnetic radiation. Use of PPTT for the purpose of cancer treatment has been widely studied as a minimally invasive and cost effective treatment modality [9]. For PPTT it is advantageous to utilize nanoparticles that transduce light to heat energy most efficiently at wavelengths of light that allow for the deepest penetration of blood and soft tissues. The near-infrared light region (800-1200 nm) offers good penetration, but gold and silver nanostructures such as nanospheres, nanocubes, and core-shell structures cannot reach surface plasmon resonance (SPR) peaks of these wavelengths, thus requiring a different approach. One such approach is to modify the geometric shape, and thus plasmon resonance of the nanoparticles. Gold nanorods (GNRs) for example, can be tuned to have SPR peaks from the visible range into the near-IR by increasing the length to width aspect ratio [10]. Another approach is to create hollow nanoparticles and vary the wall thickness and porosity to obtain the desired SPR peak, such as in gold nanocages (GNCs) [11].

Due to the challenging nature of creating hollow nanoparticles with controlled wall thickness and porosity, PPTT using such nanoparticle types has not been readily available until recently. Advancements made in the galvanic replacement reaction in which silver nanostructures serve as templates for hollow gold nanostructures with controllable size, wall thickness, and porosity has made way for the possibility of structures such as the gold nanocage to be utilized in cancer diagnostics and therapy [12].

The use of anticancer drugs within nano-based carriers offers a means of solubilizing and delivering hydrophobic drugs to the tumor site, as well as reducing distribution to other organs, and lowering the associated systemic toxicity [13, 14]. The delivery of these drugs to solid tumors relies on the nanoscale size, which reduces the uptake into healthy tissues and takes advantage of the loose junctions between vascular endothelial cells in tumors, a phenomenon known as the enhanced permeability and retention (EPR) effect [15, 16]. After permeation of the tumor, contact with receptors expressed on cancer cell surfaces can immobilize the nano-based carriers and trigger endocytosis and subsequent drug release [17]. Carriers in the 5-10 nm range are cleared rapidly from the body by urinary excretion, lessening the concerns of chronic toxicity and reducing uptake by healthy tissues. This also reduces tumor accumulation via EPR however, due to the reduced period of bioavailability [18]. With this in mind, there is a need to maximize polymeric delivery to the tumor within the bioavailability time period.

Current techniques for inducing hyperthermia, such as radiofrequency, ultrasound, or intraperitoneal perfusion are restrictive in their capacity and offer minimal selectivity toward cancerous tissues [19]. Hyperthermia induced by light absorption of plasmonic gold nanostructures allows for targeted, tissue specific localized heating. When light of a wavelength matching the SPR of the gold nanostructure interacts with the gold nanostructures, oscillations of the metallic electrons allow the light to be absorbed and for heat energy to be produced [20]. Nanostructures delivered to cancerous tissues via EPR can then be used to induce localized, tissue specific hyperthermia [21]. Our research group has previously shown that lasers can be used with gold nanoparticles to guide the delivery of macromolecules [18]. Elevated intratumoral temperatures produced by PPTT result in increased blood perfusion and vascular permeability, enhancing delivery of macromolecules by up to 1.8 fold [22]. The elevated temperatures also cause the expression of heat shock proteins that can be targeted, thereby increasing the delivery and retention of polymer therapeutics [18, 22-25]. This technique allows for temperatures ranging from mild hyperthermia at 39 °C to 45 °C up to ablative hyperthermia at 50 °C to 70 °C. Combining a mild hyperthermic macromolecular drug delivery approach with a subsequent ablative hyperthermia delivered by the same nanoconstruct system could provide for a multi-pronged therapeutic approach allowing for simultaneous ablation of tumor tissue and blocking of the macromolecules from exiting the tumor site due to damaged tumor vasculature. While these findings have shown to enhance efficacy of prostate cancer therapy in mice, little is known about the fate of the gold nanoparticles. In addition comparative effects of gold nanorods and nanocages are unknown. In this work we aim to compare the biological and physicochemical properties of GNRs and GNCs in the context of prostate tumor delivery. Factors such as cytotoxicity, uptake, ablative potential, biodistribution, acute and chronic toxicity, and efficacy of macromolecular delivery in a prostate tumor model are explored.

2. Materials and Methods

2.1 Preparation and Characterization of Nanoparticles

2.1.1 Gold Nanorod Synthesis—GNRs were synthesized using the seed-mediated growth method [26]. Optimization of silver nitrate content and the seed amount yielded

GNRs with an aspect ratio of 4.05 such that the SPR peak was 812 nm. After centrifugation and washing with deionized water, methoxy-poly (ethylene glycol) (mPEG) (5 kDa, Creative PEGWorks, Chapel Hill, NC) was added to the GNR suspension and stirred for 1 hour at a final PEG concentration of 100 μM. The mPEG GNR mixture was then dialyzed (3.5K MWCO, Spectrum Labs, Rancho Dominguez, CA) for 3 days to remove cetyltrimethylammonium bromide (CTAB) and excess unbound mPEG. The colloid was then concentrated via centrifugation.

2.1.2 Gold Nanocage Synthesis—GNCs were synthesized with an SPR peak at 810 nm using a galvanic replacement reaction between silver and gold [12]. The literature methods were modified by running 1.2 liters/min of argon across the top of the silver cube synthesis reaction to minimize oxidation effects, as well as increasing the volume size by 10 fold and running the reaction in a 250 mL round bottom flask. A 19 mm egg shaped Teflon coated magnetic stir bar was used for stirring at 350 RPMs. Temperature was held at 149°C throughout the reaction. For the galvanic exchange between gold and silver, 0.5 mL of as synthesized silver cubes were added to a 100 mL round bottom flask with 5 mL of 1 mg/mL poly(vinyl pyrrolidone) (PVP) (M_g=55,000, Aldrich). The contents were then titrated via a syringe pump at a rate of 0.8 ml/min with 0.2 mM $HAuCl_4$ to approximately 16 mL. The titration was monitored by removing small aliquots with a glass Pasteur pipette and read spectrophotometrically to determine the SPR peak. The GNCs were then washed 3 times via centrifugation with deionized water and conjugated with 5 kDa mPEG, at an equivalent concentration compared to GNRs and stirred for 1 h. The mPEG GNC mixture was then centrifuged, washed, dialyzed, and concentrated in the same manner as the nanorods.

2.1.3 Gold Nanorod and Nanocage Characterization—Characterization of the nanoparticles was performed by UV-Vis-NIR spectrophotometry (Figure 1), dynamic light scattering (DLS), and transmission electron microscopy (TEM). One hundred individual particles for each system were measured from TEM micrographs in order to obtain approximate size distributions. Due to the effect mPEG has on hydrodynamic radius, the average particle size reported by DLS was approximately 10 nm larger than that measured by TEM. The addition of mPEG to the gold nanoparticles was also found to blueshift the absorbance peak by 5-10 nm depending on the particle type. For example, the bare GNRs yielded a peak absorbance at 812 nm, whereas the mPEG bound GNRs yielded a peak absorbance at 807 nm, and had dimensions of 60 × 14.8 ± 6.5 × 2.0 nm (Figure 1). The nanorods measured zeta potential was -11.0 mV. This reaction was highly repeatable and accomplished in multi-liter batches. It was also possible to control the adsorption spectra and SPR peak by varying the silver nitrate content. The bare GNCs resulting from a galvanic exchange had a peak absorbance at 810 and the mPEG bound GNCs had a peak absorbance at 802 nm. The TEM measured particles had an edge length of 50 nm ± 7 nm (Figure 1). It was possible to tune the absorbance peak by controlling a titration of 0.2 mM $HAuCl_4$ via a syringe pump at a rate of 0.8 ml/minute. The measured zeta potential for the nanocages was -9.2 mV.

2.1.3 Comparison of Ablative Potential and ICP-MS—To compare light to heat conversion proficiency at the SPR peak, each colloidal suspension was diluted to an optical

density of 2.00. Optical density, also known as absorbance, is quantitatively expressed as $A=\log_{10}\frac{I_o}{I}$, where *Io* is the intensity of light before passing through a material and *I* is the intensity of light after it has been transmitted through the material. 5.0 mL of each colloid in a glass cuvette was irradiated with 350 mW of power from a 808 nm fiber coupled laser diode (Oclaro Inc., San Jose, CA) with collimating lens (Thorlabs, Newton, NJ) for 5 minutes. A black paper was used behind the cuvette to absorb light passing through the sample. The colloids were allowed to return to room temperature and were then irradiated again for 5 minutes two more times for three total measurements per particle type. This was to ensure that the optical properties of the particles remained stable after heating. UV-Vis spectroscopy revealed no SPR shift of either particle type after the three cycles of heating and cooling, indicating localized heating was not destroying or melting the particles at this power density. Temperatures were monitored with a Thermocouple Datalogger. Each solution was analyzed via Inductively Coupled Plasma Mass Spectrometry (ICP-MS) to determine total gold content.

To compare each of the temperature trends a correlation coefficient was calculated using the Pearson Product-Moment Correlation Coefficient given by $r=\frac{\sum(x-\overline{x})(y-\overline{y})}{\sqrt{\sum((x-\overline{x})^2\sum(y-\overline{y})^2}}$ where x and $\bar{y}$ are sample means of the two arrays of values and where r being close to 1 or -1 indicates a strong positive or negative correlation respectively.

2.2 In Vitro Uptake and Cytotoxicity

The in vitro uptake was evaluated in DU145 prostate cancer cells and human umbilical vein endothelial cells (HUVEC). The cells were plated on sterile cover slips coated with fibronectin and allowed to grow until 50% confluence. The growth media was then replaced with either 1.0 OD GNRs or 1.0 OD GNCs in the correct media. The DU145 cells were cultured in Eagle's Minimum Essential Medium with Earle's Balanced Salt Solution (ATC) supplemented with 10% fetal bovine serum (FBS) (Thermo Sceintific HyClone, Logan, UT, USA). The HUVEC cells were cultured in Clonetics Endothelial Cell Basal Medium-2 supplemented with 2% FBS, hydrocortisone, hFGF-B, VEGF, R3-IGF-1, ascorbic acid, hEGF, GA-1000, and heparin (Lonza EGM-2 BulletKit 2, Allendale, NJ, USA). The cells were then incubated for 24 hours. All cells were cultured at 37 °C in 100% humidity with 5% CO_2, kept within logarithmic growth, and kept under 10 passages. Following the incubation period, the growth medium was aspirated and the cells were washed with phosphate buffered saline followed by fixation for 10 minutes with 4% paraformaldehyde before mounting to a slide with mounting medium. The slides were imaged with an Olympus BX41 darkfield microscope coupled to a CytoViva 150 Ultra Resolution Imaging System (CytoViva, Auburn, AL, USA) using a 100× oil objective. While individual nanoconstructs are not observable utilizing this method due to optical resolution limitations, accumulations of gold were visible in both cell lines. To quantify the amount of nanoparticle uptake, pixel counting was utilized with an ImageJ pixel counting plugin (NIH) where colored pixels above a baseline threshold were counted. This method has been validated previously in our lab via ICP-MS [27].

2.2.1 Binding and Uptake in DU145 and HUVEC Cells—To compare the two nanoparticle type's uptake difference in each cell type, unpaired T-tests were utilized for both the DU145 and HUVEC data sets where each value represented the number of pixels counted per cell. The unpaired T-test tests the null hypothesis that the population means related to two independent random samples from an approximately normal distribution are equal.

2.2.2 Cytotoxicity in DU145 cells—Cytotoxicity was evaluated in DU145 cells. The cells were incubated for 48 hours in a 96 well plate (3×10^3 cells per well) at 37 °C in 100% humidity and 5% CO_2. Three wells of cells were used per OD and particle type. Following incubation with gold nanoparticles at optical densities ranging between 0 and 12, cell viability was determined using an MTT assay. This assay is a colorimetric enzyme dependent reduction of tetrazolium dye MTT 3-(4,5-dimethylthiazol-2-yl)-2,5-diphenyltetrazolium bromide to its insoluble formazan, which has a purple color.

The data set was analyzed in two different ways. First, by breaking the data down into optical density (OD) groupings and then comparing the GNRs vs the GNCs at that specific OD. This analysis was done with a T-test, as was performed the binding and uptake study, where a new T-test was performed at each OD to determine if there was a statistical difference between the GNCs and GNRs at any of the individual ODs. Next, an analysis of variance (ANOVA) with a confidence interval of 95% was performed on the whole data set to determine if the changes in percent viability as OD increased were statistically significant.

2.3 In Vivo Macromolecular Delivery and Biodistribution

Due to the experimental findings that the two particle systems offer statistically equivalent heating at equivalent optical densities, for the following animal studies we chose to dose by optical density instead of mg/kg, as optical density represents a more relevant therapeutic dosage via heat generation. This means that there is 51.3% less gold mass being injected, and an order of magnitude fewer particles (Table 1) in the GNC study groups.

On average mice have 58.5 mL of blood per kg of bodyweight [28]. A typical mouse from our study weighing 35 g therefore possessed a total blood volume of approximately 2.05 mL. The optical density of injected cages and rods was 100, making the total optical density of particles in the blood stream immediately after the bolus injection 7.5 OD, which is within the range tested in vitro showing minimal toxicity.

2.3.1 In Vivo Macromolecular Delivery via Localized PPTT—Anesthetized 8-12 week old athymic nu/nu female mice were separated randomly into groups of n=3 and subcutaneously injected with 10^7 DU145 cells in 200 μl of saline on each flank and tumors were allowed to grow until approximately 7 mm in diameter. Animals were then individually weighed and administered 150-200 μl (contingent on animal weight) of 100 OD mPEG GNRs at 8.0 mg/kg, 150-200 μl of 100 OD mPEG GNCs at 4.1mg/kg, or 150-200 μl of saline solution via tail vein injections. After 24 hours to allow for nanoparticle accumulation in the tumor, the mice were anesthetized and the tumors were swabbed with 50% propylene glycol to enhance laser penetration depth [29]. Evan's Blue Dye (EBD), an

azo dye with a high affinity for serum albumin, was injected intravenously via the tail vein at 10 mg/kg in 150-200 μl saline, depending on animal weight.

Tumors on the right flank only were then irradiated at 1.0 W/cm^2 for 10 minutes using an 808 nm fiber coupled laser diode (Oclaro Inc., San Jose, CA) with collimating lens (Thorlabs, Newton, NJ). Intratumoral temperature was monitored using a 33 gauge needle thermocouple (Omega, Stamford, CT). After 10 minutes of radiation, the laser was turned off and tumors were allowed to cool. The left tumor did not receive laser treatment to serve as an internal control. After this treatment the animals were allowed to rest for 5 hours, enough time for the EBD to be cleared from the blood [30]. The animals were then sacrificed via CO_2 inhalation. Both tumors were collected, weighed, and the EBD was extracted in 1.5 ml of formamide for 48 hrs at 60°C. The EBD content was then measured spectrophotometrically at 620 nm and divided by the weight of the tumor. The extravasation of EBD was then calculated as a ratio of the right (treated) to left (untreated) tumor and expressed as a thermal enhancement ratio (TER).

For the statistical analysis of the difference in temperature trends measured, a correlation coefficient was calculated as described in the comparison of ablative potential and ICP-MS section. For the thermal enhancement ratio it was important to show that A) there was a difference between nanoparticles being present vs. not being present, so A T-test was performed between the nanocages and the Laser alone treatment groups, and B) whether the enhancement was statistically different between the two nanoparticle types, so another T-test was performed between these two data sets.

2.3.2 In Vivo Biodistribution in Xenograft Prostate Tumor-Bearing Mice—In order to track the GNR and GNC distributions in the body, as well as the tumoral accumulation over time, their biodistribution was evaluated in prostate tumor bearing mice. Anesthetized 10-14 week old athymic nu/nu female mice were separated randomly into groups of n=5 and subcutaneously injected with 10^7 DU145 cells in 200 μl of saline on each flank and tumors were allowed to grow until approximately 7 mm in diameter. Animals were then weighed and administered 150-200 μl of mPEG GNRs at an optical density of 100 (8 mg/kg), 150-200 μl of mPEG GNCs at an optical density of 100 (4.1 mg/kg), or 150-200 μl of phosphate buffered saline via tail vein injections. Animals were then allowed to rest for 6, 24, or 72 hours. The animals were sacrificed by CO_2 inhalation, and immediately necropsied. The blood and organs from each animal were weighed and subsequently placed into polypropylene digestion tubes. Heparin was utilized to keep the blood from coagulating.

2.3.3 In Vivo Biodistribution in Mice at 7 and 28 Days—In order to evaluate the biodistribution of each nanoparticle type, and to determine whether excretion of the nanoconstructs was occurring, a 28 day study was conducted. Due to tumoral growth rates and the length of the experiment, no tumors were xenografted in this study to prevent undue discomfort to the animals. Six month old female CD1 mice were separated randomly into groups of n=5. The mice were weighed and injected via tail vein with 150-200 μl of 100 OD mPEG GNRs, 150-200 μl of 100 OD mPEG GNCs, or 150-200 μl of a saline solution as a control with weight dictating the volume injected. Animals were then left in metabolic cages to allow for collection of feces and urine. Feces and urine were collected and each animal's

weight was recorded daily. At the end of 7 days the animals were sacrificed with CO_2 and the blood was immediately drawn with a pre-heparinized needle and placed into a pre-heparinized collection tube. During necropsy the principle organs (liver, spleen, lung, kidney, heart, and brain) were removed, and the carcasses (bone, muscles and skin) were collected. Each individual sample was weighed and placed into polypropylene digestion tubes upon necropsy. This entire process was then repeated with new groups of n=5 over a 28 day collection period before necropsy and subsequent digestion.

2.3.4 Digestion and Gold Content Determination of Biodistribution Samples—

The biodistribution samples from the tumor-bearing, 7 day, and 28 day metabolic animals were each digested in aqua regia individually three times at 90 °C. Aqua regia was made from trace metal (<1 ppb) hydrochloric acid and trace metal nitric acid to avoid sample contamination with trace amounts of gold. After digestion via heat and aqua regia, each of the samples was then dried completely, and re-suspended in 5% HNO_3. The determination of gold was performed using a quadrupole ICP-MS Agilent 7500ce. An external calibration was freshly prepared from 1,000 mg/L Au solution in HNO_3 (Inorganic Ventures). Both the samples and the calibration solutions were prepared in 5 % HNO_3 (BDH Aristair Plus). A double-pass spray chamber with PTFE 100 mL/min nebulizer, platinum cones and sapphire shielded torch were used to introduce the solutions in the mass spectrometer. The instrument was located in a filtered air positive pressure lab and sample handling and chemistry was performed in laminar flow benches.

3. Results and discussions

Gold nanorod synthesis has become fairly established in the last twenty years, with strong interest in nanorod synthesis starting in the late 1990's with Y. Yu's utilization of electrochemical reduction in the presence of cetyltrimethylammonium bromide (CTAB) to form gold nanoparticles [31]. Interest and applications for gold nanorods have escalated dramatically since then, as is evident by the nearly 20,000 published scientific articles mentioning “gold nanorods” in the last two decades. As extensive research has taken place regarding control over shape and size of the particles by Murphy [32], Wang [31] and others, synthesis of high quality gold nanorods is now readily achieved in laboratory environments across the world.

Gold nanocage synthesis is still a fairly recent development however, with the first synthesis papers appearing in 2005 by Younan Xia and coworkers [33]. As such, much characterization still needs to be done in order to realize the potentials that the gold nanocage nanoconstruct hold. Once these potentials are realized we will be able to determine which applications gold nanocages will be most suited for. The work outlined in this paper set out to perform some of this necessary characterization by comparing optical, ablative, uptake, cytotoxic, tumoral macromolecular delivery and biodistribution properties to those of gold nanorods.

3.1 Characterization of Nanoparticles

Through UV-Vis-NIR spectrophotometry we showed that despite the differing shapes and sizes of gold nanorods and nanocages, we were able to obtain similar SPR peaks (Figure 1).

It is interesting to note that the SPR peaks for both the nanocages and nanorods are much sharper than that of the dielectric silica core covered by a thin gold shell, such as the nanoparticles synthesized by Loo [8], allowing for much higher specificity.

Temperature changes over time were found to be statistically equivalent, with both solutions having an average ΔT of 4 °C/min at 350 mW/cm^2. Figure 2 represents the collected data from the three consecutive heating cycles from room temperature for each particle type. These results show that light absorbed is being converted to heat at a similar efficiency for both particle systems at equivalent optical densities, as the optical density is representative of the amount of absorbance and scattering. Inductively coupled plasma mass spectrometry (ICP-MS) revealed that although the optical density and heating profiles were equivalent, gold nanorods at an OD of 2.0 contained 160 μg/mL of gold, whereas the nanocages at an OD 2.0 contained 82 μg/mL of gold. This means for equivalent light to heat transduction, gold nanocages require only 51.3% of the gold mass when compared to nanorods. This may in part be accounted for the hollow nature of the GNCs when compared to the GNRs, allowing for more surface area per gram of gold, but is most probably effected by the fact that gold nanoparticle-light interactions are highly influenced by shape and light polarization. For instance, nanorods are mainly excited by light traveling parallel to the long axis [34, 35], whereas nanocages being similar across each face can be excited along each of its axes.

If we approximate the volume of a GNR by treating the two ends as half spheres, and the middle section as a cylinder, for the synthesized GNRs the total volume of gold per GNR would be 9.72×10^{-24} m^3. With the density of gold being 19.3 g/cm^3, this means there is an average mass of 1.88×10^{-16} g per GNR. If we approximate from the TEMs that the GNC's wall thickness is 5 nm, that each of the corners is truncated 5 nm, and estimate conservatively that 50% of the interior is hollow, then the total volume of gold per GNC would be 9.20×10^{-23} m^3, or 1.78×10^{-15} g per GNC. This means that there is an order of magnitude difference between the mass of gold in one GNR versus one GNC. Using our ICP-MS data, this results in 4.26×10^{11} GNRs per mL at OD 1.0, and 2.31×10^{10} GNCs per mL at OD 1.0. These results are summarized in Table 1. This marked difference led us to believe that there may be different biocompatibility and biodistribution profiles due not only to shape differences, but also differences in particle quantity and total gold mass being delivered at equivalent therapeutic doses.

3.2 In Vitro Uptake and Cytotoxicity

As binding and uptake of the particles are dependent upon size, shape, charge, surface chemistry, and cell type, it was important for us to quantify both the uptake and cytotoxicity for each of these nanoparticles. It was observed that there was a difference in uptake dependent upon particle type and cell type (Figure 3). HUVEC cells took up the gold nanoparticles to a slightly higher degree than DU145 cells. Further, gold nanocages were taken up to a greater degree than gold nanorods in DU145 cells.

From an average of three uptake studies, it was found that the GNCs were taken up to a 28% greater extent on average than the GNRs in DU145 cells with a p-value of 0.0187, indicating a significant difference (Figure 3), where Pixels on the y-axis is the number of counted

pixels reflecting light per cell after a baseline subtraction for any reflectance observed in the control cells. In HUVEC cells GNCs were taken up 18% more than GNRs, and both nanoparticles were taken up to a greater extent than in DU145 cells indicating a slight cell dependent uptake, but a p-value of 0.145 reveals a non-significant difference between GNRs and GNCs in the HUVEC cell line.

As PEG and gold typically exhibit low toxicity on their own, a cytotoxicity study was performed to help ensure that our centrifugation and dialysis steps sufficiently removed any toxic solvents and byproducts of the nanoparticle syntheses, and to ensure that the shapes themselves did cause significantly different amounts of toxicity. Figure 4 shows that there is little statistical difference between GNRs or GNCs in terms of viability, and minimal cytotoxicity from OD 0 to 12. These results fall in line with those of others exploring cytotoxicity of gold nanoparticles showing that gold nanoparticles are “non-toxic” based on the MTT assay [36-38]. As seen by us and others, CTAB and PVP must be thoroughly removed from Au nanorods and Au nanocages respectively, and PEG or similar polymers must be utilized on the surface of the nanoparticles in order to achieve these low levels of cytotoxicity [37, 39, 40].

3.3 In Vivo Macromolecular Delivery via Localized PPTT

The animals exhibited no signs of distress or toxicity after injection of either of the mPEG gold nanoparticle systems. In the control saline group, laser alone provided between 1.0 and 2.0 °C temperature increases over 10 minutes, and was used as a baseline to determine the thermal enhancement of the gold nanoparticle systems. In Figure 5, the average temperature increase from the saline control group with laser alone has been subtracted. Post sacrificial tumor extractions revealed that the tumor and surrounding fascia was colored in EBD to a greater degree than surrounding tissues. Quantification of the EBD in the PPTT treated vs untreated tumors has been expressed as a ratio in Figure 6, and indicates that GNCs and GNRs do enhance the delivery of macromolecules. The thermal enhancement ratio of laser alone was 1.06, where a ratio of 1.00 would signify no difference between the left and right tumors, indicating negligible increase in tumor microvascular permeability. The average thermal enhancement ratios for nanocages and nanorods were 1.55, and 1.59 respectively.

In this study we found that there were similar heating and macromolecular delivery profiles for both particle types, despite the order of magnitude fewer particles in the gold nanocage groups. The ability to reduce the particle count and gold mass used in a therapy is very attractive, and warrants further exploration in terms of acute and chronic toxicity. Due to the slight differences in macromolecular delivery and heating profiles, despite similar heating profiles in solution, we hypothesized that the biodistribution of the particle types also varied and further exploration in terms of biodistribution were also warranted.

3.4 In Vivo Biodistribution in Xenograft Prostate Tumor-Bearing Mice

Results indicate that approximately 20.5% of the original injected dose of GNRs was still circulating in the blood at 6 hours, but that by 24 hours GNRs were nearly undetectable in the blood (Figure 6). Nanocage blood distribution differed slightly over this time, with 13.8% of the original injected dose of GNCs still circulating in the blood at 6 hours and

negligible amounts present at 24 hours. This indicates that the mPEG coating was effective, as bare gold nanoparticles are quickly bound by plasma proteins to form large aggregates and are cleared from the blood within minutes [41, 42]. The slight differences in blood circulation times may simply be accounted for by the order of magnitude difference in particle count, or the shape of the particles resulting in different organ level filtration. Accumulations in the heart and lungs for either particle type are negligible and seem to steadily decrease to near baseline levels after only 72 hours. Kidney accumulation for both particle types peak at 24 hours, where 1.8% of the injected GNR dose and 0.9% of the GNC injected dose accumulate in the kidneys. Spleen accumulation for both particle types is the most significant, rising initially from 6 to 24 hours, but declining by 72 hours, with GNCs clearing from the spleen at a faster rate between 24 and 72 hours. Liver accumulation trends for the two particle types is dissimilar however, with GNRs increasing out to the 72 hour time point whereas GNCs decrease in the liver from 24 to 72 hours. As the concentration of GNRs in the blood is negligible after 24 hours, despite changes in organ gold concentrations, it is our hypothesis that the lymphatic system is playing a role in nanoparticle transport, particularly when the high spleen accumulation is taken into account. Finally, tumor accumulation for nanorods seems to peak in the first few hours whereas for nanocages it peaks around 24 hours. However the accumulations at 6 and 24 hours for either particle type are not statistically significantly different. Summing the total collected mass of gold at 6 hours and 72 hours reveals a 1% drop in GNR mass, and a marked 81.3% drop in GNC mass. Note that the values reported in Figure 6 are in μg of gold per gram of tissue allowing for a better visualization of the difference in total gold present in each organ for the nanorod and nanocage groups.

It is realized that there are multiple prostate tumor cell lines (DU-145, PC3, LNCaP) and tumor models currently being used and investigated experimentally. It is also appreciated that the xenograft of human tumors has advantages as well as disadvantages [43, 44]. Due to the advantages of providing realistic heterogeneity of the tumor cells, ease of tumor extraction, ease of monitoring tumor size, cost effectiveness of the model, and our lab's experience, we chose the xenograft model but recognize that each specific tumor type and anatomical location will have differing tumor microenvironments and vascularization. The chosen model exhibits that there are significant differences in the uptake and residence time in each of the organs, and that one shape may be preferential for specific tumor microenvironment and vasculature. These results also correlate well with previous studies in athymic mice with flank xenografts of the MDA-MB-435 cell line, where it was shown that the liver and spleen take up the majority of nanorod and nanocage particles with the blood being mostly clear of particles by 24 hours [37].

3.5 In Vivo Biodistribution in Mice at 7 and 28 Days

It was observed that accumulations of both nanoparticles dropped from 7 to 28 days in the liver and spleen, and they were excreted in the feces and urine up to 28.8% of the injected dose (ID) for GNRs, and 44.3% for the GNCs (Figure 7). The lung, kidney, heart, brain and blood combined contained less than 1% of the injected dose for either GNRs or GNCs. An important difference to note between the two distributions is that accumulations in the carcass (bone, muscle and skin) appear to drop in the GNC group, as opposed to the GNR

group's increase over the 28 day period. Total recovery of gold from the animals was 91.5% for GNRs and 92.2% for GNCs.

Currently, inducing hyperthermia in the narrow window (42°C ≤ T ≤ 43°C) that provides optimal blood perfusion and permeability without causing severe vascular damage [38] is difficult in clinical settings, and non-specific heating of surrounding healthy tissues may increase non-specific drug delivery inducing undesired toxicity. PPTT possesses the ability to deliver precise thermal dosages in a highly targeted manner, potentially increasing tumor drug delivery and decreasing undesired toxicity.

Given the much lower acute and chronic nanoparticle exposure due to the lower gold mass and particle quantity needed by GNCs when compared to GNRs, as well as the significant biodistribution differences resulting in GNCs to be excreted at a higher rate, these studies have shown that gold nanocages have promising potential, and provide unique advantages compared to gold nanorods such as reduced accumulation of gold mass in tissues while providing similar heating effect, as well as the ability to load bioactive agents in their hollow structure. Each of these particle types were proven useful as mild hyperthermic agents for selective tumor heating and subsequent drug delivery and targeting, and both were still being excreted from the body at 28 days with minimal toxicity or distress observed in the animals. In addition to daily veterinarian observations for distress, the animal's weights were tracked throughout the course of the study to ensure they were eating properly and not under any undue stress or illness. Weight data has been included in Figure S1 in the supplemental data section.

4. Conclusions

We have studied gold nanorods and nanocages for their light to heat transduction efficiencies, in vitro cytotoxicity and uptake, enhancement of macromolecular delivery by plasmonic photothermal therapy, and for their biodistribution profiles. It was observed that gold nanocages are highly efficient light to heat transducers and require 18.4 times fewer particles and half the mass of gold to cause an equivalent temperature rise at a given laser intensity when compared to gold nanorods. Differences in cellular uptake were observed for both cell types and nanoparticle types with gold nanocages being taken up to a greater degree than gold nanorods, and HUVEC cells taking up more nanoparticles than DU145. Both nanoparticles offered therapeutically relevant heating capabilities and significant macromolecular delivery enhancements. Gold nanocages offered a more optimal biodistribution profile over time, with a higher excretion rate. These results point to the unique advantages of gold nanocages in plasmonic photothermal therapy and enhancement of macromolecular drug delivery.

Supplementary Material

Refer to Web version on PubMed Central for supplementary material.

Acknowledgments

The authors thank Diego Fernandez for his ICP-MS support, Nancy Chandler for her TEM support and give a special thanks to Adam Gormley for assisting with editing. Support for this project was provided by NIH grant R01 ES024681 and the Nanotechnology Training Program at the University of Utah.

References

1. Liu X, et al. A one-step homogeneous immunoassay for cancer biomarker detection using gold nanoparticle probes coupled with dynamic light scattering. J Am Chem Soc. 2008; 130(9):2780–2. [PubMed: 18257576]
2. Cheng Y, et al. Highly efficient drug delivery with gold nanoparticle vectors for in vivo photodynamic therapy of cancer. J Am Chem Soc. 2008; 130(32):10643–7. [PubMed: 18642918]
3. Kim D, Jeong YY, Jon S. A drug-loaded aptamer-gold nanoparticle bioconjugate for combined CT imaging and therapy of prostate cancer. ACS Nano. 2010; 4(7):3689–96. [PubMed: 20550178]
4. Howlander, N.; N, A.; K, M.; Garshell, J.; Miller, D.; Altekruse, SF.; Kosary, CL.; Yu, M.; Ruhl, J.; Tatalovich, Z.; Mariotto, A.; Lewis, DR.; Chen, HS.; Feuer, EJ.; Cronin, KA. SEER Cancer Statistics Review, 1975-2012. 2015. Available from: http://seer.cancer.gov/csr/1975_2012/
5. Prostate Cancer. 2015. cited 2015; Available from: http://www.cancer.org/cancer/prostatecancer/detailedguide/prostate-cancer-treating-general-info
6. Lewis, R. Surgery prices are elusive. 2014. cited 2015; Available from: http://now.uiowa.edu/2014/06/surgery-prices-are-elusive
7. Cooperberg MR, et al. Primary treatments for clinically localised prostate cancer: a comprehensive lifetime cost-utility analysis. BJU Int. 2013; 111(3):437–50. [PubMed: 23279038]
8. Loo C, et al. Immunotargeted nanoshells for integrated cancer imaging and therapy. Nano Lett. 2005; 5(4):709–11. [PubMed: 15826113]
9. Amin Z, et al. Hepatic metastases: interstitial laser photocoagulation with real-time US monitoring and dynamic CT evaluation of treatment. Radiology. 1993; 187(2):339–47. [PubMed: 8475270]
10. Murphy CJ, N R. Controlling the Aspect Ratio of Inorganic Nanorods and Nanowires. Advanced Materials. 2002; 14(1):80–82.
11. West JL, Halas NJ. Engineered nanomaterials for biophotonics applications: improving sensing, imaging, and therapeutics. Annu Rev Biomed Eng. 2003; 5:285–92. [PubMed: 14527314]
12. Skrabalak SE, et al. Facile synthesis of Ag nanocubes and Au nanocages. Nat Protoc. 2007; 2(9): 2182–90. [PubMed: 17853874]
13. Duncan R. The dawning era of polymer therapeutics. Nat Rev Drug Discov. 2003; 2(5):347–60. [PubMed: 12750738]
14. Peer D, et al. Nanocarriers as an emerging platform for cancer therapy. Nat Nanotechnol. 2007; 2(12):751–60. [PubMed: 18654426]
15. Hobbs SK, et al. Regulation of transport pathways in tumor vessels: role of tumor type and microenvironment. Proc Natl Acad Sci U S A. 1998; 95(8):4607–12. [PubMed: 9539785]
16. Matsumura Y, Maeda H. A new concept for macromolecular therapeutics in cancer chemotherapy: mechanism of tumoritropic accumulation of proteins and the antitumor agent smancs. Cancer Res. 1986; 46(12 Pt 1):6387–92. [PubMed: 2946403]
17. Lammers T, Hennink WE, Storm G. Tumour-targeted nanomedicines: principles and practice. Br J Cancer. 2008; 99(3):392–7. [PubMed: 18648371]
18. Gormley AJ, et al. Guided Delivery of Polymer Therapeutics Using Plasmonic Photothermal Therapy. Nano Today. 2012; 7(3):158–167. [PubMed: 22737178]
19. Wust P, et al. Hyperthermia in combined treatment of cancer. Lancet Oncol. 2002; 3(8):487–97. [PubMed: 12147435]
20. Link S, W Z, El-Sayed M. Alloy formation of gold-silver nanoparticles and the dependence of the plasmon absorption on their composition. Journal of Physical Chemistry. 1999; 103(18):3529–3533.

21. Huang X, et al. Plasmonic photothermal therapy (PPTT) using gold nanoparticles. Lasers Med Sci. 2008; 23(3):217–28. [PubMed: 17674122]
22. Gormley AJ, et al. Gold nanorod mediated plasmonic photothermal therapy: a tool to enhance macromolecular delivery. Int J Pharm. 2011; 415(1-2):315–8. [PubMed: 21669265]
23. Larson N, et al. Synergistic enhancement of cancer therapy using a combination of heat shock protein targeted HPMA copolymer-drug conjugates and gold nanorod induced hyperthermia. J Control Release. 2013; 170(1):41–50. [PubMed: 23602864]
24. Buckway B, et al. Gold nanorod-mediated hyperthermia enhances the efficacy of HPMA copolymer-90Y conjugates in treatment of prostate tumors. Nucl Med Biol. 2014; 41(3):282–9. [PubMed: 24461626]
25. Frazier N, et al. Effects of heating temperature and duration by gold nanorod mediated plasmonic photothermal therapy on copolymer accumulation in tumor tissue. Mol Pharm. 2015; 12(5):1605–14. [PubMed: 25839226]
26. Nikoobakht B, El-Sayed MA. Preparation and Growth Mechanism of Gold Nanorods (NRs) Using Seed-Mediated Growth Method. Chemistry of Materials. 2003; 15(10):1957–1962.
27. Gormley AJ, et al. Biological evaluation of RGDfK-gold nanorod conjugates for prostate cancer treatment. J Drug Target. 2011; 19(10):915–24. [PubMed: 22082105]
28. Mouse: Decision tree for blood sampling. cited 2015; Available from: https://www.nc3rs.org.uk/mouse-decision-tree-blood-sampling
29. Diagaradjane P, et al. Modulation of in vivo tumor radiation response via gold nanoshell-mediated vascular-focused hyperthermia: characterizing an integrated antihypoxic and localized vascular disrupting targeting strategy. Nano Lett. 2008; 8(5):1492–500. [PubMed: 18412402]
30. Kopecek J, Kopeckova P. HPMA copolymers: origins, early developments, present, and future. Adv Drug Deliv Rev. 2010; 62(2):122–49. [PubMed: 19919846]
31. Yu, et al. Gold Nanorods: Electrochemical Synthesis and Optical Properties. The Journal of Physical Chemistry B. 1997; 101(34):6661–6664.
32. Gole A, Murphy CJ. Seed-Mediated Synthesis of Gold Nanorods:? Role of the Size and Nature of the Seed. Chemistry of Materials. 2004; 16(19):3633–3640.
33. Wiley B, et al. Shape-Controlled Synthesis of Silver and Gold Nanostructures. MRS Bulletin. 2005; 30(05):356–361.
34. Sönnichsen C, Alivisatos AP. Gold Nanorods as Novel Nonbleaching Plasmon-Based Orientation Sensors for Polarized Single-Particle Microscopy. Nano Letters. 2005; 5(2):301–304. [PubMed: 15794615]
35. Wei H, et al. Polarization dependence of surface-enhanced Raman scattering in gold nanoparticle-nanowire systems. Nano Lett. 2008; 8(8):2497–502. [PubMed: 18624393]
36. Connor EE, et al. Gold nanoparticles are taken up by human cells but do not cause acute cytotoxicity. Small. 2005; 1(3):325–7. [PubMed: 17193451]
37. Wang Y, et al. Comparison study of gold nanohexapods, nanorods, and nanocages for photothermal cancer treatment. ACS Nano. 2013; 7(3):2068–77. [PubMed: 23383982]
38. Grabinski C, et al. Effect of gold nanorod surface chemistry on cellular response. ACS Nano. 2011; 5(4):2870–9. [PubMed: 21405102]
39. Ghandehari AAMH. Cellular uptake and toxicity of gold nanoparticles in prostate cancer cells: a comparative study of rods and spheres. Applied Toxicology. 2009; 30(3):212–217.
40. Gormley A, G H. Evaluation of Toxicity of Nanostructures in Biological Systems. Nanotoxicity. 2009:115–159.
41. Zhang F, et al. Gold nanoparticles decorated with oligo(ethylene glycol) thiols: kinetics of colloid aggregation driven by depletion forces. Eur Biophys J. 2008; 37(5):551–61. [PubMed: 18183382]
42. Otsuka H, Nagasaki Y, Kataoka K. PEGylated nanoparticles for biological and pharmaceutical applications. Adv Drug Deliv Rev. 2003; 55(3):403–19. [PubMed: 12628324]
43. Richmond A, Su Y. Mouse xenograft models vs GEM models for human cancer therapeutics. Dis Model Mech. 2008; 1(2-3):78–82. [PubMed: 19048064]
44. Sebastiano, V.; Donna, B. Animal Tumor Models Shared Resource. cited 2015; Available from: https://cancer.stanford.edu/research/core/Animal_Tumor.html

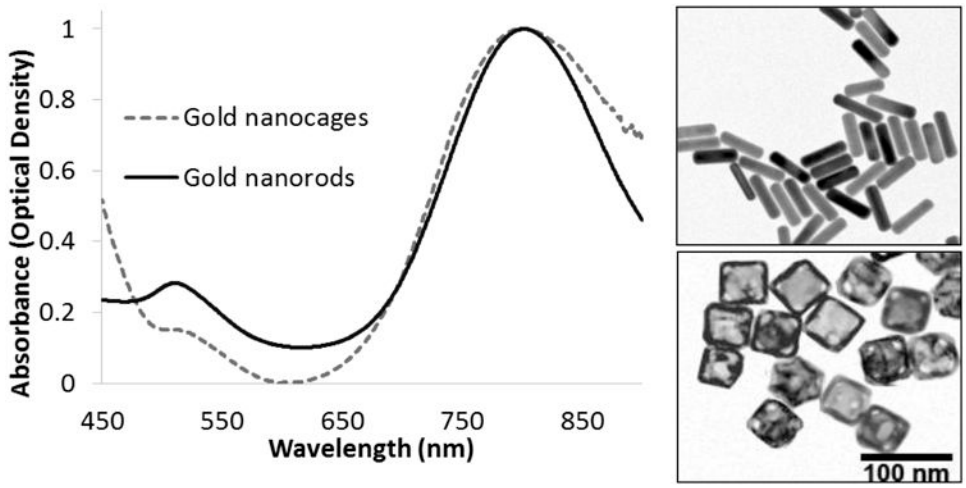

Figure 1.

Gold nanorod and gold nanocage absorbance spectrum. Optical densities at peak SPR were matched via dilution from stock solutions for easier comparison of overall absorbance spectrum. TEM of Nanorods and Nanocages. TEM image of GNRs (top) with length and width of 60 × 14.8 ± 6.5 × 2.0 nm. TEM image of GNCs (bottom) with edge length of 50 ± 7 nm, 100nm. The scale bar applies to both TEMs.

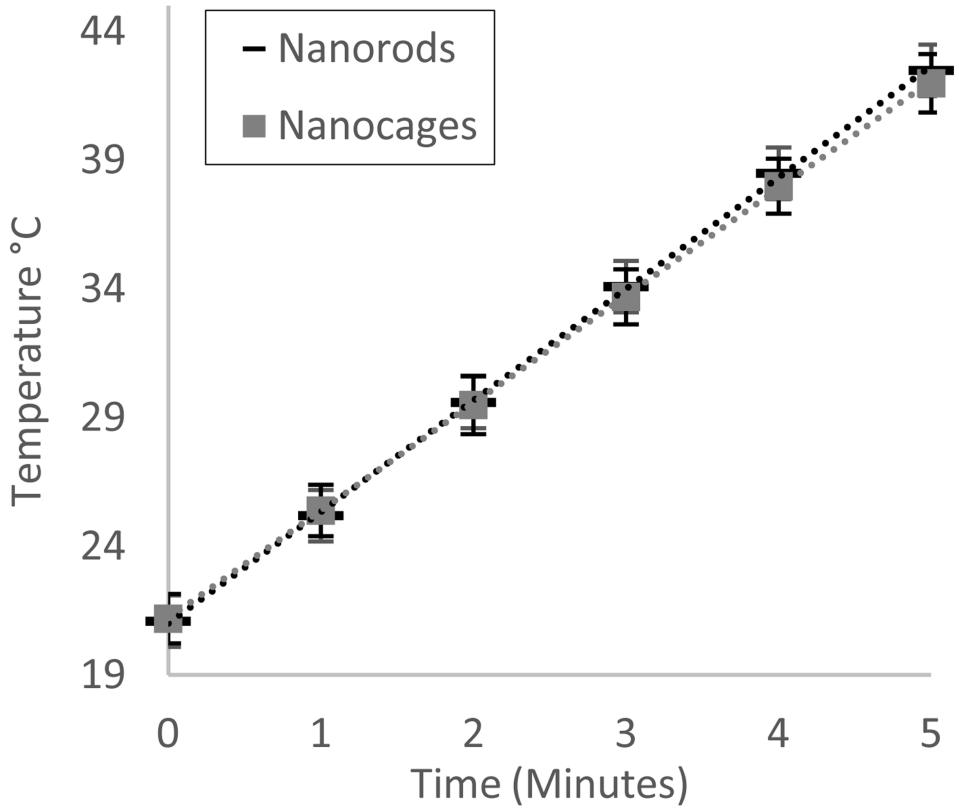

Figure 2.

Using a 350 mW 808 nm laser, 5 mL of GNR and GNC colloids were irradiated for 5 minutes, n = 3 times each from room temperature. Light-to-heat transduction for both particle types at OD 2.0 was revealed to be statistically equivalent with a correlation coefficient of 0.9999.

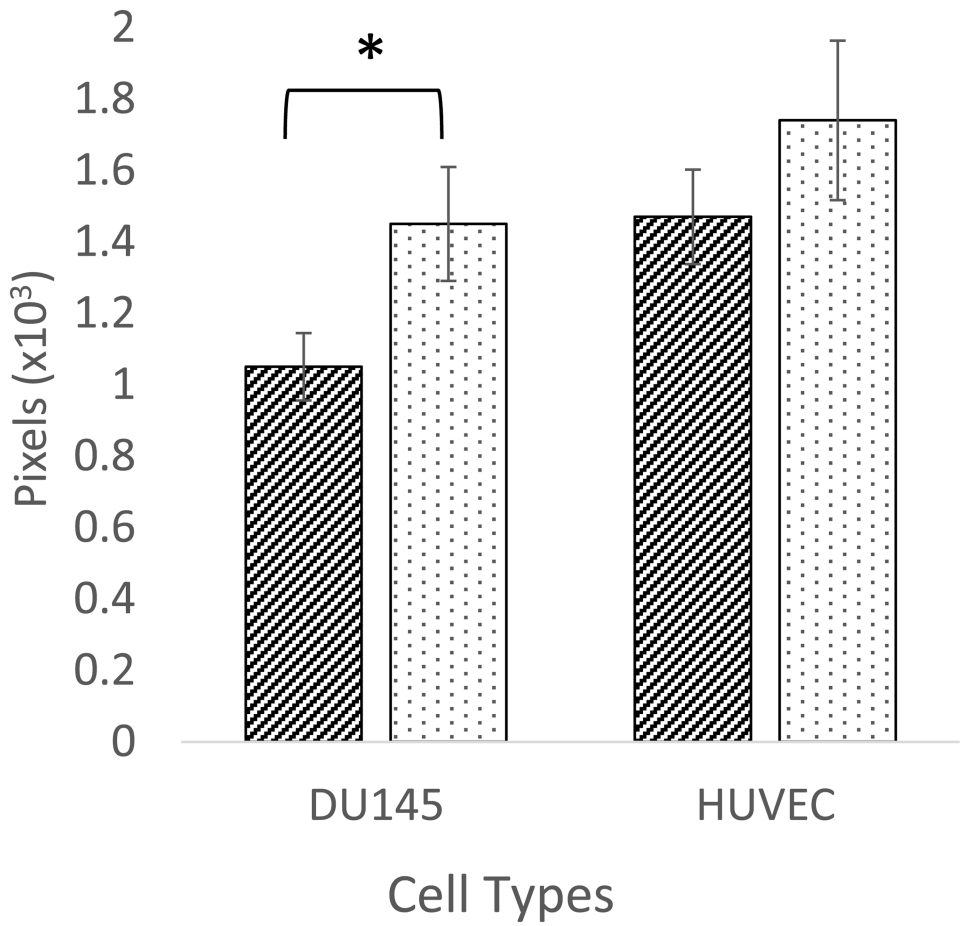

Figure 3.

Uptake of GNRs and GNCs in DU145and HUVEC cell lines. Uptake of GNCs is significantly greater than GNRs in DU145 cells (n = 3 wells, paired T-test p-value of 0.0187). Uptake in HUVEC cell was again higher with GNCs, but a non-significant difference (n = 3 wells and a unpaired T-test p-value of 0.145).

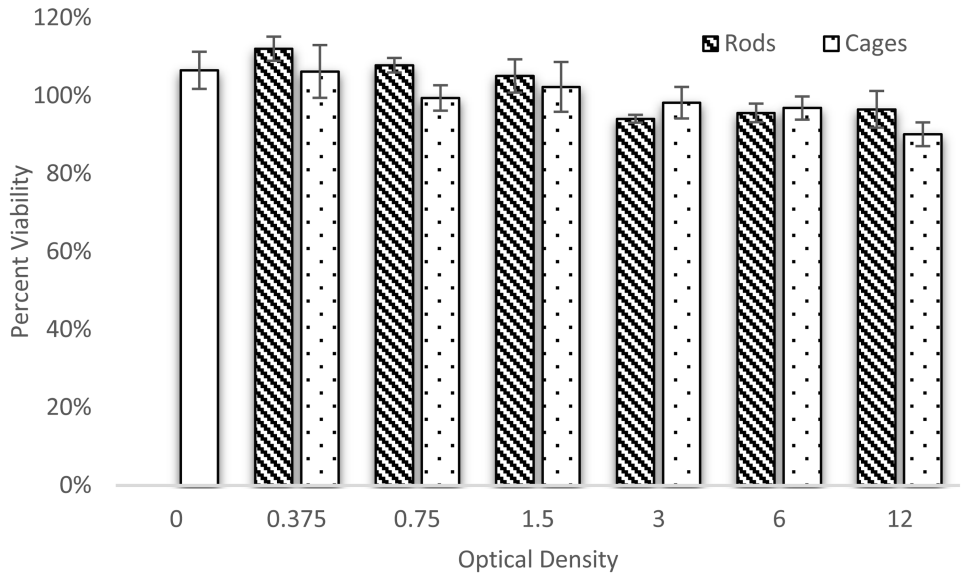

Figure 4.

Cytotoxicity of gold nanorods and nanocages in DU145 cells. Each data point represents the average and standard deviation of 3 wells of a 96 well plate. Overall there was little difference between the nanoparticle types and minimal toxicity even up to an optical density of 12. Paired T-tests at each optical density revealed all P values were > 0.1, indicating a non-significance at each optical density. Analysis of variance (ANOVA) with a confidence interval of 95% revealed again, that all P values were >0.1, indicating a non-significance across the range of optical densities.

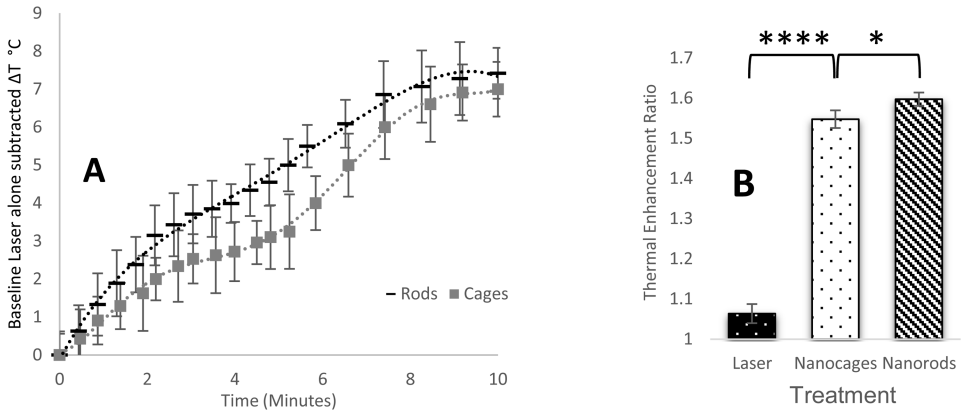

Figure 5.

A) Temperature increase as a function of nanoparticle type over ten minutes. Slight differences in the tumor heating profile when compared to that of the particles in solution alone indicate there may be differences in tumor uptake, however, both particle types achieved therapeutically relevant temperatures, and were statistically equivalent at the 10 minute mark. (n = 3 animals for each nanoparticle type, correlation coefficient = 0.975) **B)** Evan's Blue Dye delivery thermal enhancement ratio. GNRs and GNCs achieved significant enhancement of macromolecular delivery when compared to laser alone. (n = 3 animals for each treatment, a T-test between the nanocages and Laser treatment groups yields a P-value of <0.0001.) The nanoparticles were also statistically different from each other, (n = 3, a T-test between the Nanocage and Nanorod groups yields a P-value of 0.038).

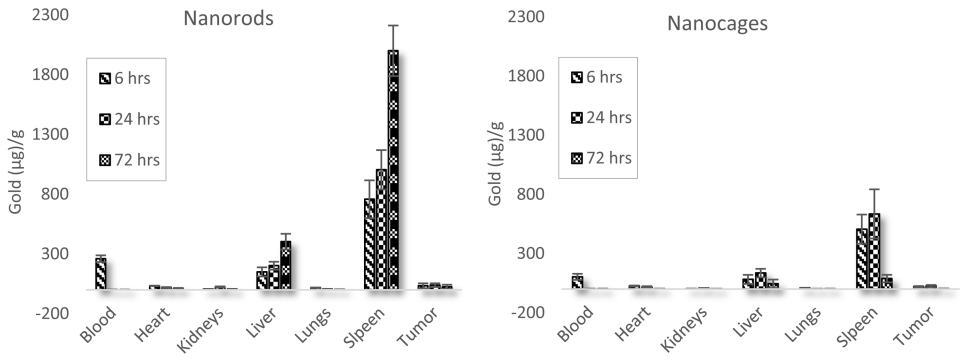

Figure 6.

Gold nanorod and nanocage biodistribution in nu/nu mice with xenografted prostate cancer tumors reported in µg of gold per g of tissue. (n = 5 for each subgroup)

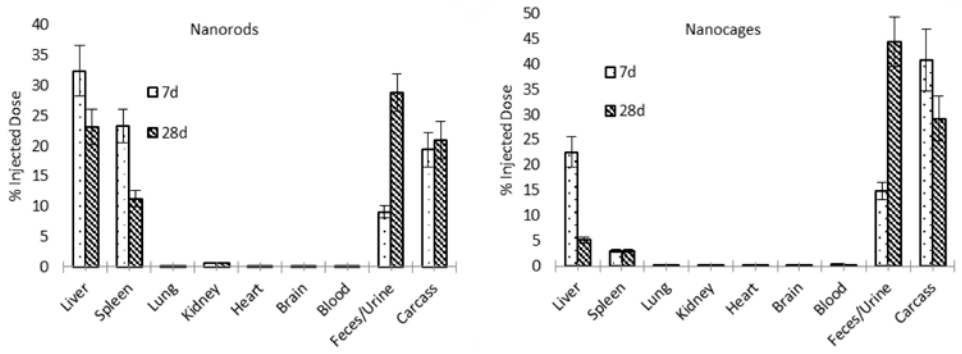

Figure 7.

Biodistribution of gold nanorods and nanocages at 7 days and 28 days, including feces and urine collection. (n = 5 for each subgroup)

Table 1

Physicochemical characteristics of GNRs and GNCs

Type	Size (nm)	mPEG bound SPR	Charge	μg/mL at OD 1.0	Particles/mL at OD 1.0
Nanorod	60 ± 6.5 × 14.± 2965+99+	807m	-11.0 mV	80	4.26×10^{11}
Nanocage	50 × 50 × 50 7	8 nm	-9.2 mV	41	2.31×10^{10}